Equation of state, phase transitions, and band-gap closure in math xmlns="http://www.w3.org/1998/Math/MathML">mrow>mi>Pb/mi>msub>mi>Cl/mi>mn>2/mn>/msub>/mrow>/math> and math xmlns="http://www.w3.org/1998/Math/MathML">mrow>mi>Sn/mi>msub>mi>Cl/mi>mn>2/mn>/msub>/mrow>/math>

T. J. Smart, E. F. O'Bannon, III, M. R. Diamond, S. Stackhouse, B. K. Godwal, Q. Williams, and R. Jeanloz

Phys. Rev. B **107**, 134113 — Published 20 April 2023

DOI: 10.1103/PhysRevB.107.134113

Equation of state, phase transitions, and band-gap closure in $PbCl_2$ and $SnCl_2$: a joint experimental and theoretical study

T. J. Smart[1], E. F. O'Bannon III[2], M. R. Diamond[1], S. Stackhouse[3], B. K. Godwal[1], Q. Williams[4], and R. Jeanloz[1]

[1] Department of Earth and Planetary Science, University of California, Berkeley, California, 94720-4767, USA
[2] Physics Division, Physical & Life Sciences Directorate, Lawrence Livermore National Laboratory, Livermore, CA 94551, USA
[3] School of Earth and Environment, University of Leeds, LS2 9JT, United Kingdom
[4] Department of Earth and Planetary Sciences, University of California, Santa Cruz, California 95064, USA

The equations of state and band gap closures for $PbCl_2$ and $SnCl_2$ were studied using both experimental and theoretical methods. We measured the volume of both materials to a maximum pressure of 70 GPa using synchrotron-based angle dispersive powder X-ray diffraction. The lattice parameters for both compounds showed anomalous changes between 16-32 GPa, providing evidence of a phase transition from the cotunnite structure to the related Co_2Si structure, in contrast to the post-cotunnite structure as previously suggested. First principles calculations confirm this finding and predict a second phase transition to a Co_2Si-like structure between 75-110 GPa in $PbCl_2$ and 60-75 GPa in $SnCl_2$. Band gaps were measured under compression to ~70 GPa for $PbCl_2$ and ~66 GPa for $SnCl_2$ and calculated up to 200 GPa for $PbCl_2$ and 120 GPa for $SnCl_2$. We find an excellent agreement between our experimental and theoretical results when using the HSE06 hybrid functional, which suggests that this functional could reliably be used to calculate the band gap of similar AX_2 compounds. Experimental and calculated band gap results show discontinuous decreases in the band gap corresponding to phase changes to higher coordinated crystal structures, giving insight into the relationship between interatomic geometry and metallicity.

Keywords: High Pressure, AX_2 compounds, $SnCl_2$, $PbCl_2$, Metallization

I. INTRODUCTION

Understanding the relationship between atomic structure and electronic properties at high pressure is a long-standing pursuit in the fields of condensed-matter and high energy-density physics, as well as in planetary and materials sciences, with the discovery of materials having technologically important properties (e.g., ferroelectrics, superconductors) being among the motivations [1-3]. Compression can transform materials to the metallic state by way of both classical (electrostatic repulsion) and quantum (Pauli exclusion) effects favoring delocalized electron states with increased density [4, 5]. However, it is unclear how changing local atomic-packing structure (e.g., coordination number) affects metallicity, as a material transforms to more highly coordinated structures under compression. Nevertheless, we recognize that most simple metals crystallize in close-packed structures (coordination number = 12) at ambient conditions [6].

Numerous studies of insulator-to-metal transitions under pressure have focused on the AX_2 family of compounds, which draw interest from a range of fields due to their planetary and technological importance and diversity in bonding character (e.g., halides, oxides, intermetallic) [7-19]. Of particular interest is SiO_2, the archetypical rock-forming compound, whose presence is expected in the deep interiors of giant (H_2 + He), "icy" (molecular species, along with H_2 and He), and large-terrestrial (e.g., "super-Earth") planets [12,14,20].

The highest-pressure observations of AX_2 compounds (SiO_2, CaF_2) document the insulator-to-metal transition under dynamic compression, in which elevated temperatures melt the sample prior to metallization [20,21]. Notably, in at least some of these compounds (e.g., SiO_2, $AuGa_2$), nearest-neighbor coordination increases under compression while in the fluid state, following the trend displayed in solid-state structures on compression [22-24]. However, the short timescales and fluid samples

of these make typical methods of quantifying the interatomic geometry (e.g., X-ray diffraction) challenging, motivating the study of analog compounds that already have highly coordinated cations at ambient conditions to document the relationship between band gap closure and interatomic geometry.

AX_2 compounds, despite their diversity in bonding character, typically follow a sequence of predictable structural transitions on compression, with cation coordination increasing at each step (Fig. 1) [7-19]. This sequence is considered well-established up to the 9-fold coordinated cotunnite phase. High-pressure studies of AX_2 compounds that crystallize in the cotunnite phase at ambient conditions (e.g., $PbCl_2$ and $SnCl_2$) thus allow us to extend our understanding of the role of interatomic geometry on electronic and other material properties beyond the established regime.

In this study, we characterize the crystal structures, equations of state, and band gaps of $PbCl_2$ and $SnCl_2$ to pressures of over 70 GPa and compare our measurements with the results of ab-initio electronic structure calculations. Given that metallization (e.g., band-gap closure) is notoriously challenging to predict using first-principles calculations, experiments can be used to check theory, which – to the degree that it is thereby validated – can provide fruitful predictions of material properties at pressure-temperature conditions that are not accessible with current experimental techniques [25, 26].

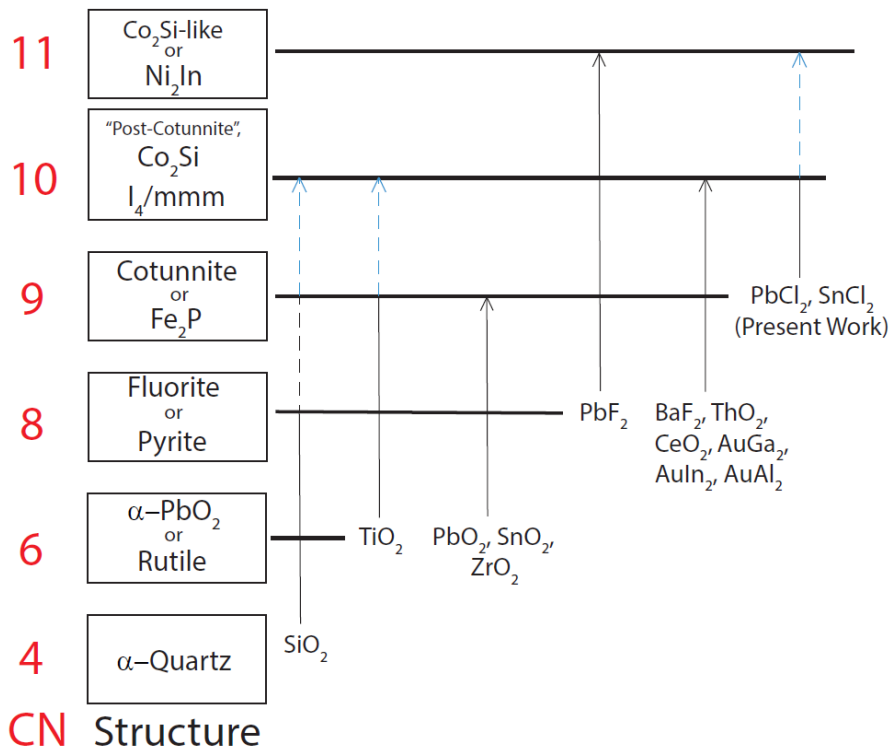

Figure 1. Crystal-structural sequence of AX_2 compounds at ambient conditions and high pressures. Figure after Leger et al. [4]. Cation coordination number (CN) of the cation is shown on the *left*, next to the structure name. Several AX_2 compounds are shown with *arrows* noting experimentally determined high-pressure phases [7-19]. *Dashed arrows* denote structures calculated from first principles, and *blue* color indicates that metallization is expected for the high-pressure phase. Several compounds (e.g., GeO_2, Na_2Te, HgF_2, $BaCl_2$, BaI_2, $BaBr_2$), and the effects of temperature are omitted for clarity.

II. METHODS

A. High-pressure experiments

Polycrystalline $PbCl_2$ and $SnCl_2$ (Sigma Aldrich >99% purity, with natural isotopic ratios) were ground to micron-sized grains and loaded into symmetric-type diamond-anvil cells, leaving ~30% void space to allow room for the

pressure medium. Diamond anvils had a culet size of 200 μm, and rhenium gaskets pre-indented to ~30μm thickness and drilled with 80μm diameter holes were used. Ruby spheres of ≤ 5 μm diameter were placed inside the sample chamber and ruby fluorescence was used to determine the pressure [27].

All experiments were conducted at room temperature: this is substantially above the Debye temperatures of these materials, as estimated from their ambient pressure vibrational spectra [28,29], and hence the presence of different isotopes is not expected to affect their high-pressure transitions at room temperature.

Samples were loaded in either a neon pressure medium, or a 16:3:1 methanol:ethanol:water pressure medium. $SnCl_2$ is hygroscopic, so it was loaded in a dry argon atmosphere. Mid-infrared spectra were collected to affirm minimal water content of $SnCl_2$ samples before all high-pressure experiments.

The band gap (absorption edge) was measured through visible and near-infrared spectroscopy. In all experiments a background measurement was collected using a fully assembled but empty diamond cell and the background was subtracted from the spectra. Optical absorption spectra were collected on a Horiba LabRam HR Evolution Raman spectrometer, with a white light source being used to collect spectra from 400-800 nm (3.1eV-1.55eV). Near-infrared spectra were collected using an evacuated Bruker Vertex 70v FTIR equipped with a tungsten source, InSb detector and CaF_2 beamsplitter [30]. Spectra were collected from 14,000 to 8,500 cm^{-1} (714.3 to 1,176.5 nm, 1.74 eV to 1.05 eV) with a resolution of 4 cm^{-1} (0.2-0.6 nm across this frequency range). As a note, though the sensor resolution is on the meV scale, we observe band gap closure in our samples on the scale of eV over 10s of GPa, indicating that the true resolution of absorption edge measurements is controlled by the resolution of our pressure measurements and is on the scale of ~0.1 eV. No pressure medium was used in the experiments to measure the band gap under pressure, and the pressure gradients in these experiments are large. However, because of the spatial resolution of our instrument and the sharpness of the absorption edge of our samples, we do not anticipate that non-hydrostatic conditions adversely affect our band-gap determinations.

Angular dispersive synchrotron X-ray diffraction experiments were performed at beamline 12.2.2 at the Advanced Light Source (Lawrence Berkeley National Laboratory), using a monochromatic X-ray beam with $\lambda = 0.4959$ Å (25 keV). A Mar345 detector collected diffracted X-rays at 331.4 (±0.1) mm. Detector distance and orientation were calibrated using a LaB_6 standard, and the diffraction images were radially integrated using the programs FIT2D [31] or Dioptas [32].

We carried out Rietveld refinements using the General Structure Analysis System (GSAS) [33] Larson program, with starting atom positions chosen from the outputs of ab-initio density functional theory described in the following section. After fitting the background, the data were refined for lattice parameters. Pseudo-Voigt functions are used for the fitting of diffraction-peak profiles in the Rietveld refinements.

B. Theoretical Calculations

All calculations were performed using the density functional theory-based VASP code, employing the projector augmented-wave method [33-37]. The potentials were generated using valence configurations of $4d^{10}\ 5s^2\ 5p^2$ for Sn, $5d^{10}\ 6s^2\ 6p^2$ for Pb, and $3s^2\ 3p^5$ for Cl. Scalar relativistic effects were accounted for. However, spin-orbit coupling was only included in the calculations for $PbCl_2$ phases because it was found to have a negligible effect on the results of calculations for $SnCl_2$ phases. Computations were performed using both the local-density approximation (LDA) and Perdew-Burke-Ernzerhof (PBE) formulation of the generalized gradient approximation (GGA) [38, 39]. The LDA and GGA give reasonable estimates of structural parameters, but underestimate band gaps (e.g., Xiao et al., 2011) [40], due to their inherently incomplete cancellation of self-interaction [25, 26]. In view of this, additional band-gap calculations were performed using the Heyd-Scuseria-Ernzerhof (HSE06) hybrid functional, which incorporates a fraction of exact-exchange to alleviate the self-interaction error, on structures optimized using the PBE

functional [41]. The HSE06 hybrid functional predicts band gaps that are in much better agreement with experimental measurements, but has a high computational cost, making it unsuitable for geometry optimizations in the present work [40, 42]. HSE06 was chosen out of the popular hybrid density functionals, because it is shown to be the most accurate in calculating the band gaps of semiconductors [42].

For geometry optimization calculations, the kinetic-energy cut-off for the plane-wave expansion was 600 eV, and Brillouin-zone sampling was performed using a 6×4×8 *k*-point grid [43]. These settings ensured calculated volumes were converged to within 0.05 $Å^3$, and enthalpies to within 1 meV per atom.

For LDA and PBE band-gap calculations, the kinetic-energy cut-off for the plane-wave expansion was 600 eV, and Brillouin-zone sampling was performed using an 11×7×15 *k*-point grid [43]. These settings ensured that calculated band gaps were converged to within about 0.05 eV or less. Due to the high computational cost associated with hybrid functional calculations, for HSE06 band gap and density of states calculations, Brillouin-zone sampling was performed using a 5×3×7 *k*-point grid [43]. Convergence tests for LDA and PBE suggest that using this smaller *k*-point grid leads to overestimates of the band gap of up to 0.05 eV for $SnCl_2$ and 0.2 eV for $PbCl_2$.

It is well known that LDA underestimates pressure, and PBE overestimates pressure. Because of this, a pressure correction was estimated using the method of Oganov et al. [44], but without a thermal pressure term (this is likely negligible at ambient temperature for these calculations performed at 0K). The calculated pressure shifts ($PbCl_2$: +2 GPa (LDA), - 2 GPa (PBE); $SnCl_2$: +2 GPa (LDA), - 1 GPa (PBE)) move the isothermal compression curves to higher or lower pressure, bringing them in better accord with experimental values.

III. RESULTS AND DISCUSSION

A. X-ray diffraction results

X-ray diffraction data were collected on compression and decompression to 71 GPa in both $PbCl_2$ and $SnCl_2$ (Fig. 2, example diffraction patterns shown in Appendix A). Rietveld refinements of the diffraction patterns for both compounds document an isosymmetric phase transition from the cotunnite structure (orthorhombic *Pnma*, 9-fold coordination) to the Co_2Si structure (orthorhombic *Pnma*, 10-fold coordination) between 17 and 35 GPa for $PbCl_2$ and 17 to 33 GPa for $SnCl_2$, supporting a prior theoretical prediction [45] (structural diagrams are shown in Fig. 4). These findings are consistent with structural transitions documented in other AX_2 compounds such as PbF_2, $BaCl_2$, and $BaBr_2$ [9,13], and the gradual nature of the transition is fully compatible with the close topological relationship between the cotunnite structure and the Co_2Si structure [46].

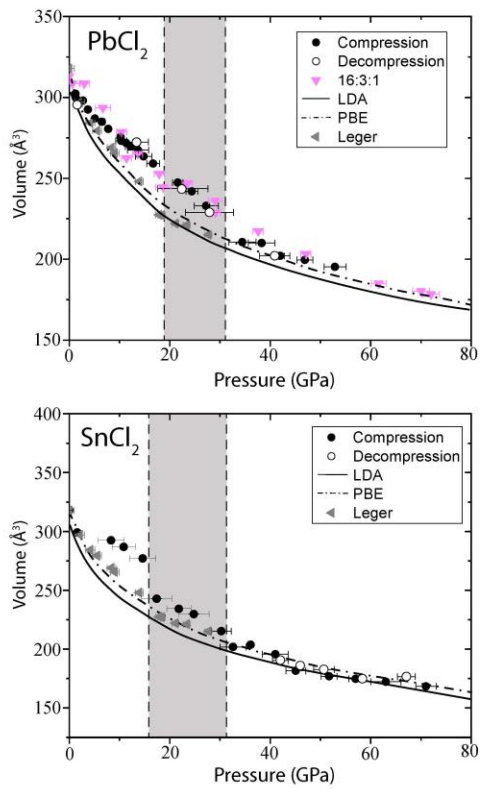

Figure 2. Pressure–volume data for $PbCl_2$ (*top*) and $SnCl_2$ (*bottom*). Data shown in *Black or hollow circles* were taken using neon pressure medium. *Pink triangles* not data taken using 16:3:1 methanol:ethanol:water pressure medium, and *grey triangles* are previous results from Leger et al. [10].The pressure-range for the transformation from cotunnite to Co_2Si structures, between 17 and 35 GPa for $PbCl_2$ and 17 and 33 GPa for $SnCl_2$, is shown by the *gray box* between *dashed lines* as it is for Figs. 3 and 8. Data collected on compression and decompression are distinguished by *closed* and *open circles*, respectively.

Measured lattice parameters provide a greater insight into the structural transition that

occurs over a relatively large pressure range for both materials. The cotunnite-to-Co_2Si transition in these materials is characterized by an anomalous shift in relative length of lattice parameters (Fig. 3) [47]. This occurs between 17 and 35 GPa for $PbCl_2$ and between 17 and 33 GPa for $SnCl_2$. In these regions we observe anisotropic compressibility of the unit cell, with a strong compression along the *a*-axis, a reduced compression along *c*-, and *extension* along *b*-, which has been reported to occur in other AX_2 compounds that transform from the cotunnite structure to the Co_2Si structure under compression (e.g., PbF_2, CeO_2, and ThO_2) [13, 18]. While we were not able to collect data on decompression in the pressure range of this phase transition in $SnCl_2$, in $PbCl_2$ the transition is observed to be reversible with minor hysteresis.

The strong compression of the *a*-axis relative to the *b*- and *c*-axes is emphasized when we normalize the lattice parameters against their respective initial lengths (Fig. 3 c and d). The pressure range of the phase transition is marked by the gray shading between dashed lines, with a smooth transition in $PbCl_2$ that is complete by 33 GPa, and a sudden shift in $SnCl_2$ at 33 GPa. Due to the non-negligible pressure gradients, we attribute this more sudden shift between phases to be a result of non-hydrostatic stresses.

Previous experiments by Leger et al. [10] did not exhibit these continuous trends in lattice parameters or the presence of an intermediate phase and had strong hysteresis on decompression (gray triangles, Figs. 2 & 3). This difference is likely associated with the more non-hydrostatic stress environments within the samples of their experiments, as these had no pressure medium for $SnCl_2$ and silicone grease for $PbCl_2$. Because of the contrast in the nature of the transition (abrupt in the previous experiments and with an intermediate zone of transformation in ours), we do not preclude that the transition from the cotunnite to the Co_2Si structure can be driven/enhanced by non-hydrostatic stresses.

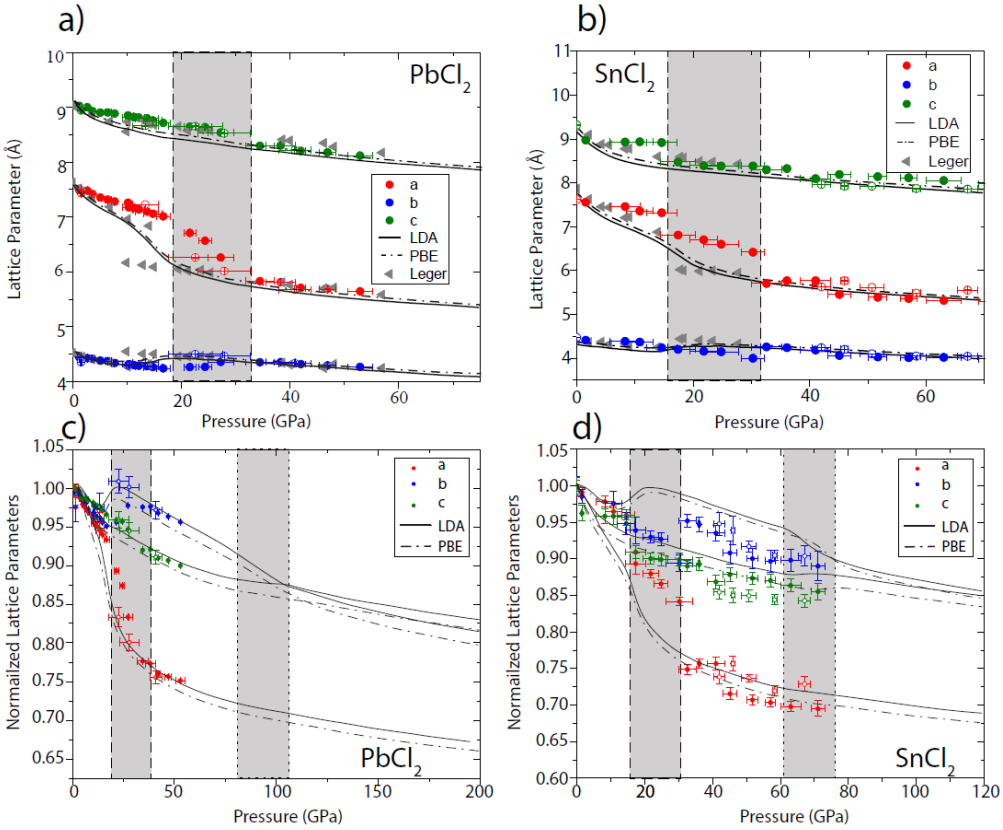

Figure 3. Lattice parameters vs. pressure from experiments and theory are presented for $PbCl_2$ (a) and $SnCl_2$ (b). Lattice parameters normalized against ambient-pressure values are presented as a function of pressure for $PbCl_2$ (c) and $SnCl_2$ (d). Lattice parameters show a gradual change in slope between 21 and 25 GPa for $PbCl_2$ and between 17 and 33 GPa for $SnCl_2$, contrasting with previous work that showed a sharp transition (*gray triangles* in a) and b)). We infer a gradual change in phase ("transition zone"), consistent with findings for other AX_2 compounds as the materials shift from the cotunnite to Co_2Si structure. We mark these transition zones with gray boxes, whose boundaries are defined by the

observed shifts in lattice parameters (*gray boxes* with *dashed black lines*). The experimentally observed compression of the *a* and *c* axes and extension of the *b* axis is reflected in calculations. Upon further compression, LDA and PBE calculations predict a distortion of the Co_2Si lattice, seen here as a slight contraction of the *b* axis and extension of the *c* axis between 75 and 110 GPa in $PbCl_2$ and between 60 and 75 GPa in $SnCl_2$, shown by the *gray box* between *dotted lines* in c) and d).

Density functional theory calculations agree well with experimental data, with compression of the *a*-axis and extension of the *b*-axis reproduced by the calculations, albeit at pressures ~10 GPa lower than experimentally observed (Figs. 2 and 3). Between 75 and 110 GPa in $PbCl_2$ and 60 and 75 GPa in $SnCl_2$, PBE and LDA functionals predict another shift in structure from the 10-fold coordinated Co_2Si structure to an 11-fold coordinated Co_2Si-like phase (structure shown in Fig. 4). This phase shares the same space group as the Co_2Si structure (*Pnma*), but the rows of atoms become increasingly colinear and orthogonal to one another, as the anion sublattice begins to approach a close-packed array. The transition is characterized by a subtle extension of the *c*-axis and compression of the *b*-axis, which has pronounced expression in the normalized lattice parameters plots (Fig. 3 c and d, *gray shading* between *dotted lines*). As has been previously noted [12], the nine-fold cation coordination of the cotunnite structure is incompatible with close-packing of the anion framework. Indeed, the cotunnite structure can be viewed as being comprised of interlinked $(MX_2)_n$ polymeric chains [48]. The sequential transitions can then be viewed as a progression from a phase characterized by high cation coordination but an inefficiently packed anion sublattice (anions coordinated in trigonal prisms) to a phase with both higher cation coordination and far more efficiently packed anions (Fig. 4 d). The transition sequence is a higher-coordination analogue to the structural shifts in the SiO_2-system at lower pressures, in which a polymeric low-pressure phase (quartz, with corner-linked SiO_4 tetrahedra) converts to the close-packed and more highly coordinated rutile structure.

Structural rearrangements from the cotunnite to Co_2Si and then to Co_2Si-like phases are shown in Fig. 4; the formation of new bonds between Pb or Sn and Cl is indicated by the *red* and *black arrows*. Electron density maps (Fig. 4 d) show that formation of the first bond (shown by the *red* and *black arrow*) occurs at 24 GPa in $PbCl_2$ and at 28 GPa in $SnCl_2$ (not shown), similar pressures to observations of analogous bonds forming in PbF_2 by Stan et al. [13]. Further compression leads to a tightly packed arrangement, with atoms forming an increasingly square lattice within each layer in the (010) plane, until the structure becomes 11-fold coordinated (Co_2Si-like structure) at 110 GPa in $PbCl_2$ and at 75 GPa in $SnCl_2$.

Reference	**Cotunnite structure**			**Co_2Si structure**			**Co_2Si-like structure**		
	V_0	**K_0**	**K_0'**	**V_0**	**K_0**	**K_0'**	**V_0**	**K_0**	**K_0'**
$PbCl_2$ This study	**313.06± 0.05**	46.7±4.4	4.8±1.2	300(20)	47.2±3.2	4.0±1.0	286(3)	59.2±0.3	4.0±0
$SnCl_2$ This Study	**318.03± 0.05**	27.9±2.1	6.3±0.5	292(43)	41.1±3.7	4.0±0.2	290(8)	43.7±0.1	4.0±0
$PbCl_2$ Ref. [10]	313.072	34±1	7.4±6	273.91	95±10	4.3±5			
$SnCl_2$ Ref. [10]	317.853	31±2	4.9±8	263.81	91±10	**4.0**			

Table 1. Comparison of our equations of state with previous work by Leger et al. [10]. Zero-pressure volume V_0, bulk modulus K_0, and pressure derivative K_0' for the high-pressure phases (Co_2Si and Co_2Si-like) are determined through 3rd order Birch Murnaghan equations of state by fitting normalized pressure to Eulerian strain (*G* vs. *g*) [49] (see Appendix B for details). The volume $\boldsymbol{V_0}$ for the ambient pressure cotunnite phase is obtained from our X-ray diffraction data via Rietveld refinement and are fixed in these fits. Equations of state for the Co2Si-like structure are determined from outputs from PBE calculations. Bold lettering indicates values that were fixed in our fits.

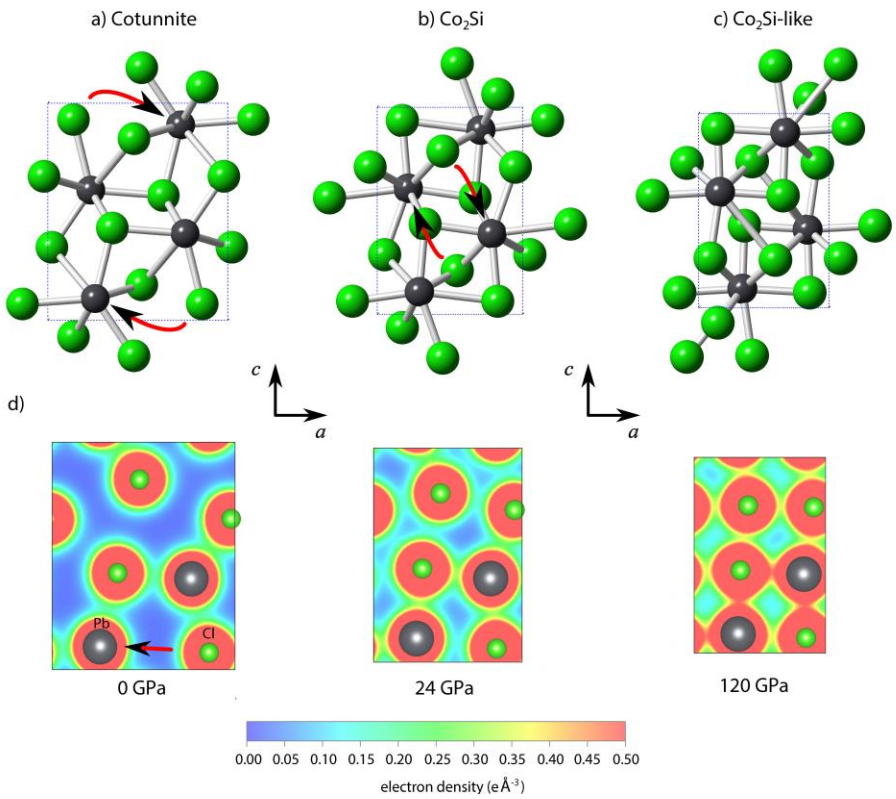

Figure 4. Structural diagrams of the cotunnite, Co_2Si, and Co_2Si-to-Co_2Si-like phases, with the Pb, Sn cations shown in *black* and chlorine shown in *green*. a), b), and c) show ball-and-stick models of the cotunnite, Co_2Si, and Co_2Si-like structures respectively, with *arrows* indicating the atomic motion that leads to new bonds in subsequent phases. d) shows the change in electron density in the (010) plane as a function of pressure. A new bond forms between Pb and Cl at 24 GPa, indicative of a transformation from the 9-fold coordinated cotunnite structure (a) to the 10-fold coordinated Co_2Si structure (b). For $SnCl_2$, formation of an analogous Sn-Cl bond is observed at about 28 GPa. On further compression the lattice continues to become more ideally packed, and new (Pb,Sn)-Cl bonds form. This Co_2Si-like structure is predicted by DFT to occur at 120 GPa in $PbCl_2$ and 80 GPa in $SnCl_2$. Figures were produced using VESTA 3 [50].

We fit our pressure-volume data with a 3rd order Birch-Murnaghan equation of state (EOS), and the obtained parameters are shown in Table 1. EOSs previously reported [10] were determined assuming a single phase, and we obtain similar results when we fit our data in this way. However, when we fit our high- and low-pressure phases separately, we find the high-pressure phase to have higher V_0 and lower bulk modulus K_0 than previously reported (fits shown in Appendix B).

B. Band-gap measurements

Representative absorption-edge spectra, collected between 30 and 70 GPa for $PbCl_2$ and between 20 and 66 GPa for $SnCl_2$, show good agreement with theory (Fig. 5 and Appendix D, Fig. 10 and Table 2). Of the three functionals used, as expected HSE06 agrees best with the experimental data, overestimating the band gap by only 0.2 eV, which is due to an incomplete convergence with respect to k-point sampling.

For $PbCl_2$ and $SnCl_2$ we observe three distinct regions in the theoretically calculated band gaps with compression. Discontinuities in the band gap vs. volume plots, and shallowing slope in the band gap vs. volume plots are attributed to changes in $PbCl_2$ and $SnCl_2$ as they transform from the cotunnite to Co_2Si phase (*gray box* with *dashed lines*) and from the Co_2Si to Co_2Si-like phase (*gray boxes* with *dotted lines*). Experimental data for $SnCl_2$ follow this trend, closely following values calculated by the HSE06 functional, at pressures and volumes coinciding with the calculated structural changes (Fig. 5 *b* & *d*).

When the experimental $PbCl_2$ data are extrapolated to zero band gap, we predict band

closure at 206 ±24 GPa, which agrees with HSE06 calculated band-gap closure at 200 GPa. When we extrapolate the experimental $SnCl_2$ data for the Co_2Si-like phase (between 51 and 66 GPa) to zero band gap, we predict band closure at 125 ±9 GPa versus 120 GPa predicted by HSE06. If, however, we extrapolate the entire $SnCl_2$ experimental data set to zero band gap, we predict band closure at 97 ±6 GPa, representing a 20 GPa discrepancy between experiments and HSE06.

The lower metallization pressure of $SnCl_2$ relative to $PbCl_2$ differs from the typical trend of metallization pressures decreasing along isoelectronic series down the periodic table to heavier, more electron-rich compounds. This trend, which is also found in band-structure calculations of other compounds [51, 52], does not predict the relative band-gap closure pressures of the two compounds examined here. This apparent inversion of metallization pressure is likely generated by the relativistic down-shift and associated localization of the 6*s* lone pair in Pb relative to the somewhat more delocalized 5*s* lone pair in Sn. Indeed, portions of the Pb 6*s* states are among the deepest in the valence band at all pressures, and the 5*s* states of Sn systematically contribute substantially more to the density of states at the top of the valence band relative to the 6*s* states in $PbCl_2$ (see Appendix E). Comparable lowering of the band gap of SnO relative to PbO via this "inert lone pair" has been extensively documented at ambient pressures [53, 54], and we demonstrate here that this 6*s*-localization persists to high pressures in the chlorides of these elements.

We observe a dramatic increase in slope in the band gap vs. volume plot at high compression (Fig. 5, *bottom panels*). During compression of the initial cotunnite phase in both compounds, we observe a small reduction in band energy predicted by HSE06 calculations (5% and 14% of ambient pressure band gap for $PbCl_2$ and $SnCl_2$ respectively), despite a significant change in unit-cell volume (roughly 50% of the total volume closure of the materials, with total volume closure $V_{tot}= V_0-V_{band\ closure}$). At the onset of the transition between 9-fold coordinated cotunnite and 10-fold coordinated Co_2Si structures, we observe a large (>20%) reduction in the band gap in both compounds, despite small reductions in unit cell volume (~14% of V_{tot}). This transition is also accompanied by a shift in the cation coordination around the anions, from 4 and 5 for the two different Cl sites in the cotunnite structure toward 5 and 6 in the Co_2Si structure (as illustrated by the new Pb-Cl bond formation in Fig. 4). Upon further compression in the Co_2Si region, the slope becomes steeper, with small changes in the unit cell volumes (~3% V_{tot}) producing large decreases in the band gap. We find a significant drop in band gap at the expected Co_2Si-to-Co_2Si-like phase boundary around 170 $Å^3$, and the $SnCl_2$ data show discontinuities corresponding to the expected phase boundaries in agreement with the calculated HSE06 results.

The observed steepening of band gap with unit-cell volume is likely due to the additive effects of compression and changes in interatomic geometry. Under compression, increased electron orbital overlap broadens the valence and conduction bands, reducing band gaps. Interatomic geometry can further increase electronic orbital overlap as pressure-induced changes in crystal structures force neighboring orbitals into proximity of each other. Recent work shows the tunability of band gaps with cation-anion bond angles, finding that the band gap decreases as the crystal structure becomes more square-like, in which electron orbitals are forced into overlapping configurations [57-59]. This is consistent with our observations on $PbCl_2$ and $SnCl_2$, in which we observe discontinuous down shifts in the band gap across the transformation from cotunnite to the progressively more close packed-like Co_2Si and Co_2Si-like structures (Fig. 4).

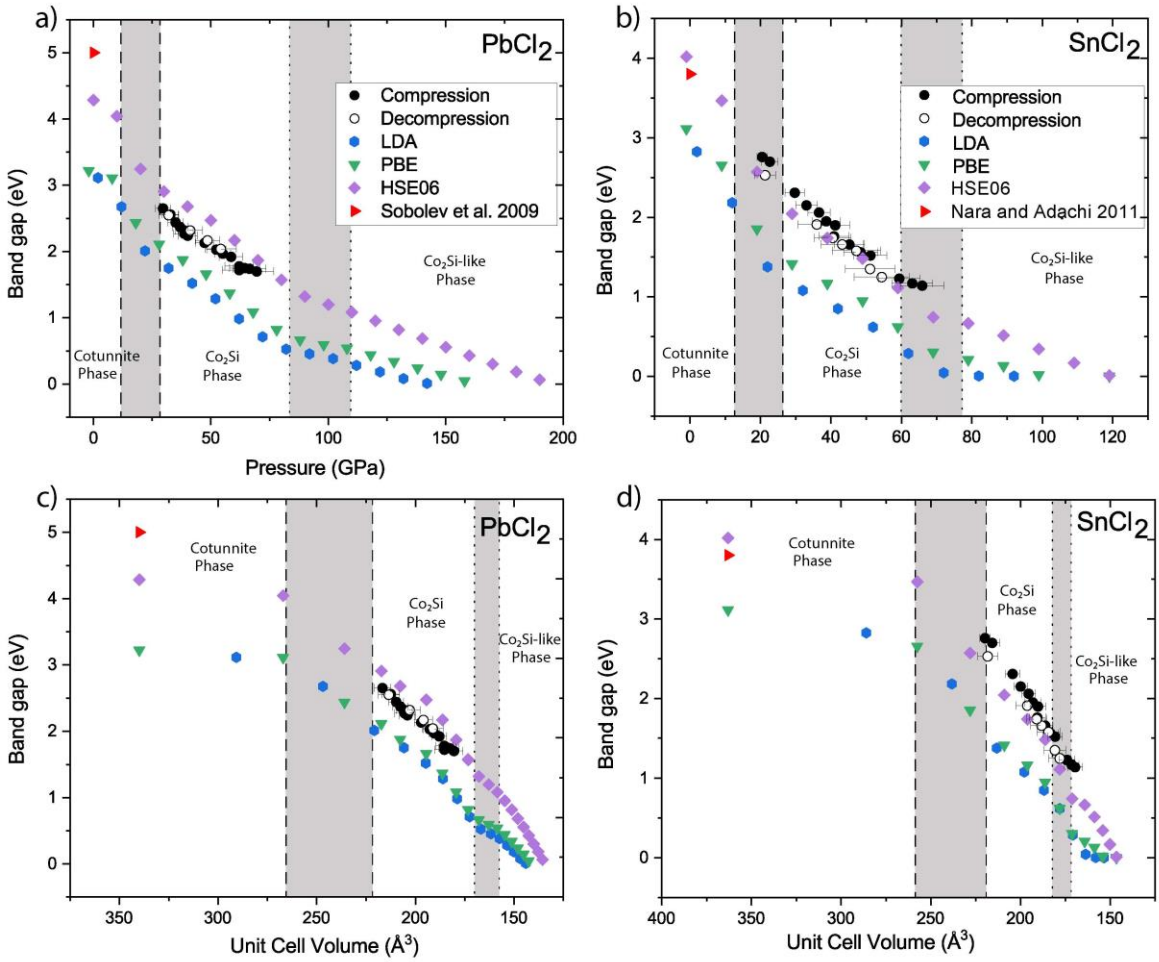

Figure 5. Band gap as a function of pressure (*top* panels) and as a function of volume (*bottom* panels) from experiment and theory for $PbCl_2$ (*left*) and $SnCl_2$ (*right*). Zero-pressure band gaps were obtained from Sobolev et al. [55] for $PbCl_2$ and Nara and Adachi [56] for $SnCl_2$. The *gray box* with *dashed lines* shows the pressure range for the transition from the 9-fold coordinated cotunnite to the 10-fold coordinated Co_2Si structure, and the *gray box* with *dotted lines* shows the pressure range for phase transformation from the Co_2Si structure to the 11-fold coordinated Co_2Si-like structure, as labeled in Figs. 2 & 3. For both $PbCl_2$ and $SnCl_2$, HSE06 fits the data better than either LDA or PBE, albeit with a small overestimation of band gap. (*top*) Extrapolation of our experimental data yields band gap closing pressures of 206 ±24 GPa for $PbCl_2$ and 97 ±6 GPa for $SnCl_2$, in reasonable agreement with theory (200 GPa and 120 GPa respectively). (*bottom*) Volumes for the experimental points are calculated using the equations-of-state model from our compression data. Around 230 $Å^3$ the slope steepens, corresponding to the emergence of the Co_2Si phase and the increase in coordination number in the crystal structure. Extrapolation of our experimental data to band-gap closure yields a closure volume of 131 ±21 $Å^3$ for $PbCl_2$ and 150 ±5 $Å^3$ in $SnCl_2$, in excellent agreement with theory (135 $Å^3$ and 146 $Å^3$ respectively).

Phrased another way, the increased shift in band gap with respect to volume at high compressions has a straightforward physical explanation: the approach to close packing of these materials as they progress through the two phase transitions, coupled with the concomitant increases in both cation and anion coordination, enhances the overlap between the cation conduction (mostly Pb 6*p* and Sn 5*p*) and anion valence (mostly Cl 3*p*) bonding states (see Appendix E). For larger volumes (lower pressures) within the cotunnite structure, the inefficient packing of the anion framework within this quasi-polymeric structure leads to a larger band gap; as the packing becomes more efficient, the rate of band gap decrease is notably enhanced.

IV. CONCLUSIONS

Static compression experiments to over 70 GPa and theoretical simulations to 200 GPa for $PbCl_2$ and 120 GPa for $SnCl_2$ show evidence of a continuous transition from the 9-fold coordinated cotunnite structure to the 10-fold coordinated Co_2Si structure between 17 and 35 GPa in both $PbCl_2$ and $SnCl_2$. Upon further compression, density functionals predict the transition to an 11-fold coordinated Co_2Si-like phase between 75 and 110 GPa in $PbCl_2$ and 60 and 80 GPa in $SnCl_2$, remaining the stable phase through the pressure range of our calculations.

Using equations of state validated by experiments, we calculate band-gap closure using the LDA, PBE, and HSE06 functionals. The hybrid functional HSE06 agrees best with our experimental data, confirming the superiority of HSE06 for calculating the electronic band structure of AX_2 compounds.

Our work shows the relationship between changing interatomic geometry and the closing of the band gap under high pressure, with applications for other AX_2 compounds in both fluid and solid states, which have been demonstrated to transition from low to high coordination number upon compression [7-19,22,23]. In particular, our results illustrate that the general pattern of phase transitions in AX_2 compounds from structures that can be viewed as polymeric to those characterized by close-packed anion packing recurs as cation coordination numbers increase under compression. In the particular case of cotunnite relative to the post-cotunnite phases, a distorted but highly coordinated cation environment and complex prismatic anion coordination forms a structure that can be viewed as composed of interlinked polymeric chains, which under compression converges on a phase that approaches close-packing. Our band gap measurements and calculations confirm that such a close-packed anion framework, coupled with high cation coordination numbers, is associated with the metallization of AX_2 oxides [14]. These results are of special interest for SiO_2, a major component of rocky planets that is predicted to exist in the cotunnite phase at pressures corresponding to super-Earth interiors [12]. Previous work investigating the band structure of SiO_2 at these conditions predicts metallization in the I4/mmm phase near 1.4 TPa, though these calculations were preformed using traditional density functionals, motivating the use of hybrid functionals like HSE06 to better constrain the high-pressure band structures [19]. Prediction of metallic SiO_2 could inform us of its potential to influence the dynamics and chemical partitioning in the deep cores of giant planets.

Acknowledgements

This work was supported by NNSA through the Center for Materials at Extreme Conditions (CMEC) consortium. E. O'Bannon and Q. Williams acknowledge support from EAR- 1620423 and the Consortium for Materials Properties Research in Earth Sciences (COMPRES) under NSF Cooperative Agreement EAR 16-06856. E. O'Bannon also acknowledges that a portion of this work was performed under the auspices of the US Department of Energy by Lawrence Livermore National Laboratory under Contract No. DE-AC52-07NA27344. The Advanced Light Source is supported by the Director, Office of Science, Office of Basic Energy Sciences, of the U.S. Department of Energy under Contract No. DE-AC02-05CH11231. S. Stackhouse was supported by Natural Environment Research Council (NERC) grant number NE/K006290/1. The calculations were performed on ARC1, ARC2, and ARC 3, part of the High-Performance Computing facilities at the University of Leeds, UK, and ARCHER, the UK's national high-performance computing service.

Appendix A: X-ray Diffraction Patterns

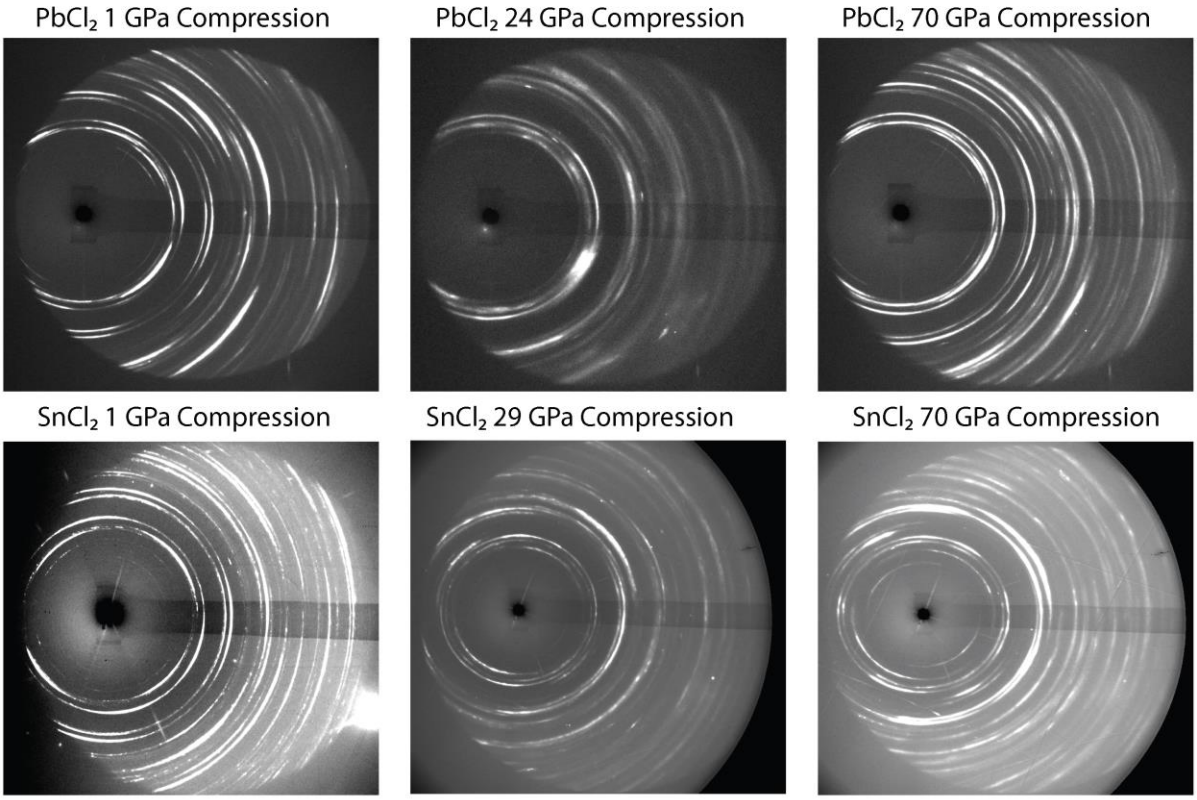

Figure 6. Raw X-ray diffraction data for $PbCl_2$ (top) and $SnCl_2$ (bottom). Patterns for the cotunnite phase (left), transitional phase (middle) and Co_2Si phase (right) are shown for each compound.

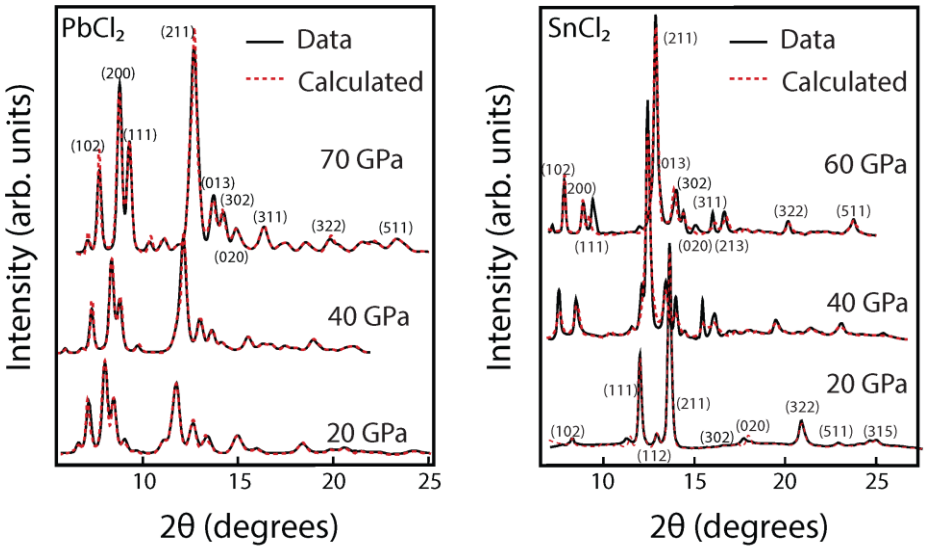

Figure 7. X-Ray diffraction patterns for $PbCl_2$ (left) and $SnCl_2$ (right). Both observed (black) and patterns calculated with Reitveld refinement (Dashed red) are shown.

Appendix B: Fits for Equations of State

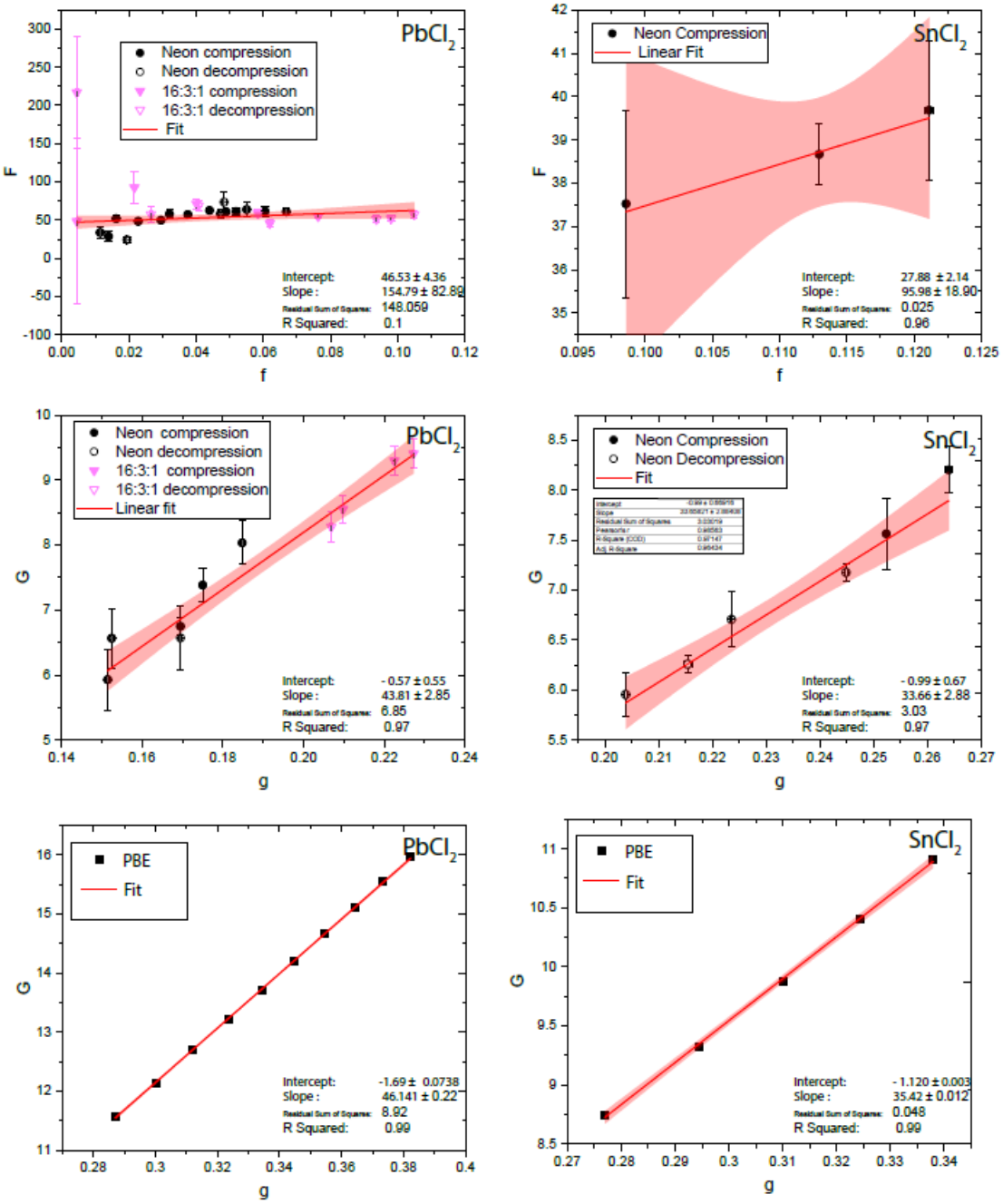

Figure 8. Eulerian strain vs. normalized strain (F vs. f)(*cotunnite phase, top*) and effective strain vs. normalized strain (G vs. g) (*Co_2Si phase, middle and Co_2Si-like phase, bottom*) are shown for $PbCl_2$ (*left*) and $SnCl_2$ (*right*). F vs. f plots were used to determine the equations of state for the low-pressure phases, while G vs. g was used for high-pressure phases [47]. Data from the phase transition zone fit neither equation of state and were thus omitted. A weighted least-squares fit was applied to each data set (red lines) and 95% confidence intervals are shown (red shading).

Appendix C: Using ratios of the lattice parameters to determine phase changes:

The transformation between the cotunnite and Co_2Si structures is characterized by a shift in the ratios of lattice parameters and a change in coordination from 9- to 10-fold. Jeitschko [47] and Leger et al. [8] show that the a/c and (a+c)/b ratios distinguish between phases with orthorhombic (*Pnma*) symmetry. These ratios were later updated by Stan et al. [13], who show that for the cotunnite structure a/c = 0.8-0.9 and $(a+c)/b$ = 3.3-4.0, and for Co_2Si a/c = 0.7-0.78 and $(a+c)/b$ = 2.90-3.56. When our data are plotted using these ratios, we see a clear distinction between the cotunnite and Co_2Si phases (Fig. 9). Points that fall between the two phases are between 17 and 27 GPa for $PbCl_2$ and 17 and 33 GPa for $SnCl_2$. LDA and PBE calculations follow experimental data closely over the pressure range of our experiments. Here, the shift to the distorted Co_2Si-like phase is seen as a strong inflection point toward higher $(a+c)/b$ values near $(a+c)/b$ = 3.2.

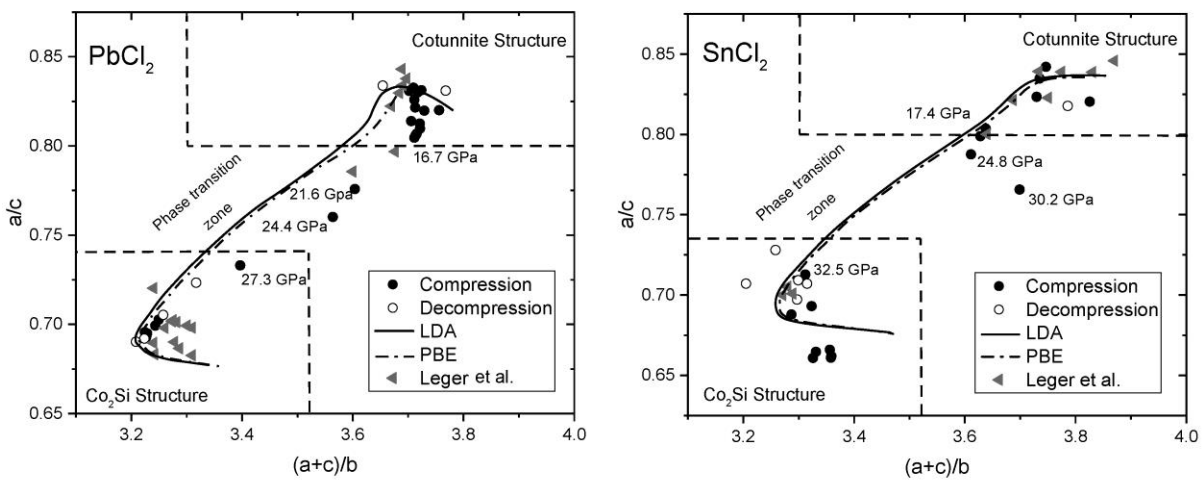

Figure 9 . Lattice parameter ratios of $PbCl_2$ (left) and $SnCl_2$ (right). Borders that define the phases follow Stan et al. [13]. Circles are data from this study, with solid circles indicating data taken on compression and empty circles those taken on decompression. Data from Leger et al. [10] are plotted as gray triangles. Calculated lattice ratios are shown as the solid (LDA) and dash-dot (PBE) curves.

Appendix D: Absoption edge spectroscopy with pressure

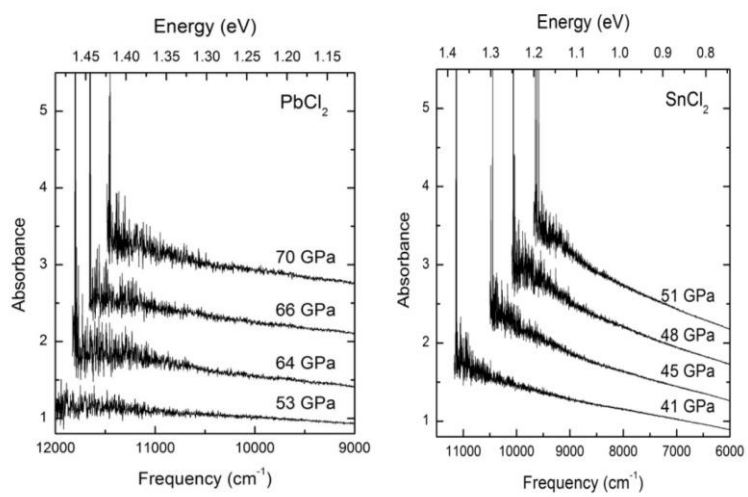

Figure 10. Representative high-pressure spectra of the absorption edge of $PbCl_2$ (a) and $SnCl_2$ (b). No exciton peaks are resolved within these experiments. These spectra show that the energy of the band gap *decreases* as pressure *increases*. Spectra are stacked for clarity.

Table 2: Absorption edge Experimental Data: Pressures, Unit Cell Volume, and Band gaps.

	Pressure (GPa)		Volume (Å^3)		Measured Band gap (eV)	Adjusted Band gap (eV)
$PbCl_2$	29.57	3.11	299.20	0.15	2.65	-
	32.78	3.5	292.50	0.10	2.56	-
	34.99	3.24	216.69	4.27	2.44	-
	36.9	3.4	212.48	4.41	2.37	-
	38.7	3.69	209.78	3.85	2.32	-
	40.16	3.97	207.57	3.86	2.24	-
	38.7	4.55	205.57	4.02	2.27	-
	47.3	3.81	204.0	4.19	2.13	-
	52.27	4.05	205.57	4.96	2.03	-
	55.07	3.36	197.04	3.46	1.97	-
	58.56	5.03	192.75	3.34	1.92	-
	62	7.2	190.50	2.64	1.72	-
	62	6.05	187.84	3.72	1.78	-
	64.3	6.33	185.37	5.05	1.45	1.75
	66.4	6.99	185.37	4.24	1.44	1.74
	69.5	7.25	183.79	4.28	1.40	1.7
	54.16	6.59	182.40	4.58	2.04	-
	48.55	5.21	180.42	4.53	2.17	-
	41.23	5.17	191.23	5.27	2.32	-
	32.02	4.22	195.92	4.62	2.55	-
$SnCl_2$	20.48	1.45	219.86	2.79	2.75	-
	22.63	2.33	215.84	4.16	2.72	-
	29.72	2.81	204.48	3.99	2.34	-
	33.08	3.01	199.89	3.89	2.18	-
	36.61	3.12	195.49	3.68	2.06	-
	38.68	3.98	193.1	4.47	1.95	-
	41.2	4.12	190.33	4.36	1.6	1.9
	40.9	4.27	190.65	4.55	1.46	1.76
	45.24	4.3	186.21	4.16	1.36	1.66
	48.4	4.85	183.23	4.4	1.26	1.56
	51.2	4.71	180.74	4.04	1.22	1.52
	59.4	5.93	174.17	4.39	0.93	1.23
	63.1	5.81	171.49	4.04	0.87	1.17
	65.9	6.21	169.58	4.13	0.84	1.14
	54.4	7.82	178.061	6.34	0.95	1.25
	51.1	7.01	180.83	6.04	1.05	1.35
	47.2	6.87	184.34	6.4	1.28	1.58
	43.2	5.99	188.24	6.08	1.36	1.66
	40.5	5.21	191.08	5.61	1.44	1.74
	36	5.4	196.23	6.5	1.91	-
	21.3	3.02	218.29	5.67	2.53	-

Table 2: Experimental Data for absorption edge measurements: Measured pressures, and volumes are shown with their values in the first column and confidence bands in the second column. Pressures were determined using the standard ruby fluorescence tech nique, and volumes were determined using the experimentally determined equations of stare. At larger bandgaps (3.1 eV-1.55 eV) the Horiba LabRam HR Evolution was used and at lower band gaps (1.74 -1.05 eV) the Bruker Vertex 70v FTIR spectrometer was used. The Horiba detects the middle of the absorption edge, and the Bruker detects the very bottom of the absorption edge, introducing an instrument-induced discontinuity in the pressure-band gap and volume-band gap trends. The band gaps of the infrared data were adjusted by comparing the last visible-light measurement and first IR measurement (62 &64.3 GPa for $PbCl_2$ and 38.7 & 40.9 GPa for $SnCl_2$) to make a correction assuming the band shape remains the same. This results in an upshift in the IR data of 0.3 eV in both compounds. Measured and adjusted band gap values are shown.

Appendix E: Density of States Calculations

The partial density of states for $PbCl_2$ & $SnCl_2$ calculated using the HSE06 exchange-correlation functional shows that the valence band has primarily Cl 3*p* and Pb, Sn 6*s* character. The unoccupied conduction band has mainly Pb, Sn 6*p* and diminished Cl 3*p* character. All bands broaden with increasing pressure, as band gap reduces from about 4 eV at ambient pressure in each $PbCl_2$ and $SnCl_2$ to closure.

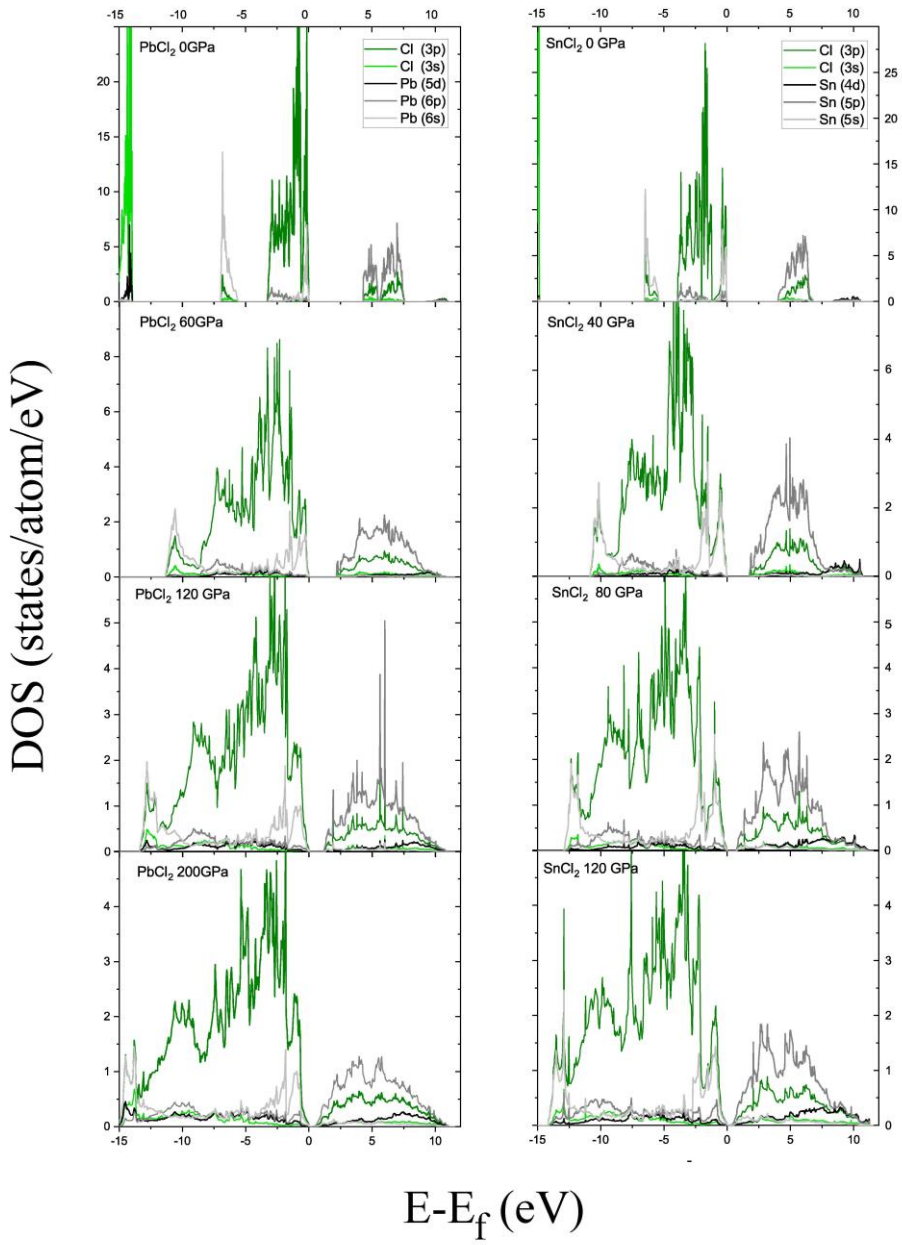

Fig 11: Calculated density of states (DOS) for $PbCl_2$ at 0, 60, 120, and 200 GPa (left) and $SnCl_2$ at 0, 40, 80, and 120 GPa (right) using HSE06 density functional. Ambient pressure DOS (*top panels*) show a clear distinction between *s* & *p* orbitals in both Pb, Sn and Cl, with an energy gap of around 4 eV. We observe a broadening of all states to higher pressure (*downward panels*).

Appendix F: Experimental Data

Table 3: Experimental Data: Pressures, Unit Cell Volume, and Lattice parameters.

	Pressure (GPa)		Volume (Å^3)		a (Å)		b (Å)		c (Å)	
$PbCl_2$	1.6	0.2	299.20	0.15	7.556	0.001	4.412	0.001	8.973	0.005
	8.3	2.6	292.50	0.10	7.459	0.002	7.000	0.004	8.935	0.004
	10.8	2.3	286.85	0.15	7.358	0.002	4.369	0.005	8.937	0.006
	14.6	2.6	277.10	0.13	7.319	0.002	4.244	0.004	8.920	0.005
	17.4	3.0	242.80	0.10	6.813	0.011	4.203	0.006	8.478	0.002
	21.8	2.4	234.31	0.10	6.707	0.001	4.162	0.001	8.394	0.001
	24.8	3.0	229.70	0.15	6.602	0.001	4.150	0.001	8.383	0.002
	30.3	4.0	215.33	0.10	6.419	0.001	4.002	0.002	8.383	0.003
	32.6	4.6	201.92	0.10	5.709	0.002	4.262	0.001	8.300	0.000
	36.1	0.3	203.70	0.10	5.770	0.002	4.241	0.001	8.325	0.003
	41.0	2.6	195.60	0.10	5.770	0.004	4.187	0.002	8.096	0.004
	45.1	2.0	181.70	0.13	5.455	0.004	4.066	0.004	8.191	0.004
	51.7	1.6	176.99	0.04	5.392	0.002	4.030	0.003	8.145	0.002
	57.0	1.4	174.82	0.05	5.365	0.002	4.015	0.004	8.117	0.003
	63.0	3.0	172.32	0.06	5.321	0.002	4.021	0.004	8.053	0.003
	71.0	2.0	168.40	0.20	5.300	0.006	3.984	0.007	7.973	0.007
	67.1	1.8	176.70	0.10	5.556	0.005	4.047	0.003	7.859	0.003
	58.3	0.7	174.92	0.10	5.486	0.002	4.051	0.000	7.870	0.000
	50.7	2.1	182.70	0.02	5.618	0.001	4.104	0.001	7.923	0.002
	46.0	0.6	185.82	0.30	5.770	0.005	4.203	0.007	7.926	0.005
	42.0	1.6	190.40	0.11	5.632	0.005	4.243	0.004	7.966	0.004
$SnCl_2$	1.6	0.2	299.20	0.15	7.556	0.001	4.412	0.001	8.973	0.005
	8.3	2.6	292.50	0.10	7.459	0.002	7.000	0.004	8.935	0.004
	10.8	2.3	286.85	0.15	7.358	0.002	4.369	0.005	8.937	0.006
	14.6	2.6	277.10	0.13	7.319	0.002	4.244	0.004	8.920	0.005
	17.4	3.0	242.80	0.10	6.813	0.011	4.203	0.006	8.478	0.002
	21.8	2.4	234.31	0.10	6.707	0.001	4.162	0.001	8.394	0.001
	24.8	3.0	229.70	0.15	6.602	0.001	4.150	0.001	8.383	0.002
	30.3	4.0	215.33	0.10	6.419	0.001	4.002	0.002	8.383	0.003
	32.6	2.6	201.92	0.10	5.709	0.002	4.262	0.001	8.300	0.000
	36.1	0.3	203.70	0.10	5.770	0.002	4.241	0.001	8.325	0.003
	41.0	2.6	195.60	0.10	5.770	0.004	4.187	0.002	8.096	0.004
	45.1	2.0	181.70	0.13	5.455	0.004	4.066	0.004	8.191	0.004
	51.7	1.6	176.99	0.04	5.392	0.002	4.030	0.003	8.145	0.002
	57.0	1.4	174.82	0.05	5.365	0.002	4.015	0.004	8.117	0.003
	63.0	3.0	172.32	0.06	5.321	0.002	4.021	0.004	8.053	0.003
	71.0	2.0	168.40	0.20	5.300	0.006	3.984	0.007	7.973	0.007
	67.1	1.8	176.70	0.10	5.556	0.005	4.047	0.003	7.859	0.003
	58.3	0.7	174.92	0.10	5.486	0.002	4.051	0.000	7.870	0.000
	50.7	2.1	182.70	0.02	5.618	0.001	4.104	0.001	7.923	0.002
	46.0	0.6	185.82	0.30	5.770	0.005	4.203	0.007	7.926	0.005
	42.0	1.6	190.40	0.11	5.632	0.005	4.243	0.004	7.966	0.004
	0.0	0.0	318.03	0.05	7.623	0.002	4.476	0.003	9.322	0.006

Table 3: Experimental Data: Measured pressures, volumes and lattice parameters for $SnCl_2$ and $PbCl_2$ on compression and decompression. The determined value for each measured parameter is shown in the first column, and the confidence band is shown in the second column. Volumes and lattice parameters were obtained though Rietveld refinement of our XRD data. At each pressure step we measured pressure in several locations determined using the standard ruby fluorescence technique [27]. Pressures reported are the median pressure, and the error bars represent the total range of deviation from median pressure for a given pressure step.

References

[1] N. F. Mott, *Metal-Insulator Transitions*, (CRC Press) (London) (1990)

[2] Young, David A.. *Phase Diagrams of the Elements*, (University of California Press) (Berkeley) (1991)

[3] C. J. Pickard, I. Errea, M.I. Eremets., Annual Review of Condensed Matter Physics 11, 57 (2020)

[4] L. Stixrude and R. Jeanloz, Proceedings of the National Academy of Sciences of the United States of America 105, 11071 (2008).

[5] P. M. Celliers, P. Loubeyre, J. H. Eggert, S. Brygoo, R. S. McWilliams, D. G. Hicks, T. R. Boehly, R. Jeanloz and G.W. Collins, Physical Review Letters 104, 184503 (2010).

[6] L. Pauling, The Nature of the Chemical Bond 3rd Edition, (Cornell University Press), (Ithaca New York), (1960)

[7] J. M. Leger, J. Haines, and A. Atouf, Journal of Applied Crystallography 28, 416 (1995).

[8] J. M. Leger, J. Haines, A. Atouf, O. Schulte, and S. Hull, Physical Review B 52, 13247 (1995).

[9] J. M. Leger, J. Haines, and A. Atouf, Physical Review B 51, 3902 (1995).

[10] J. M. Leger, J. Haines, and A. Atouf, Journal of Physics and Chemistry of Solids 57, 7 (1996).

[11] J. Haines, J. M. Leger, and O. Schulte, Journal of Physics-Condensed Matter 8, 1631 (1996).

[12] A. R. Oganov, M. J. Gillan, and G. D. Price, Physical Review B 71, 8, 064104 (2005).

[13] C. V. Stan, R. Dutta, C. E. White, V. Prakapenka, and T. S. Duffy, Physical Review B 94, 12, 024104 (2016).

[14] M. J. Lyle, C. J. Pickard, and R. J. Needs, Proceedings of the National Academy of Sciences of the United States of America 112, 6898 (2015).

[15] O. Ohtaka, D. Andrault, P. Bouvier, E. Schultz, and M. Mezouar, Journal of Applied Crystallography 38, 727 (2005).

[16] S. R. Shieh, A. Kubo, T. S. Duffy, V. B. Prakapenka, and G. Shen, Physical Review B 73, 7, 014105 (2006).

[17] S. J. Duclos, Y. K. Vohra, A. L. Ruoff, A. Jayaraman, and G. P. Espinosa, Physical Review B 38, 7755 (1988).

[18] H. X. Song, L. Liu, H. Y. Geng, and Q. Wu, Physical Review B 87, 9, 184103 (2013).

[19] S. Duwal, C.A. McCoy, P.F. Weck, P. Kalita, H. L. Hanshaw, K. Cochrane, T. Ao, S. Root, Physical Review B 102 024105 (2020)

[20] M. Millot, N. Dubrovinskaia, A. Cernok, S. Blaha, L. Dubrovinsky, D.G. Braun, P.M. Celliers, G.W. Collins, J.H. Eggert, R. Jeanloz, Science 347, 418 (2015).

[21] H. Shu, Y. Zhang, B. Wang, H. Dong, T Tobase, J. Ye, X. Huang, S. Fu, T. Sekine., Physics of Plasmas 27, 4, 030701 (2020).

[22] B. Kalkan, B. Godwal, S. V. Raju, and R. Jeanloz, Scientific Reports 8, 10, 6844 (2018).

[23] A. Denoeud, S. Mazevet, F. Guyot, F. Dorchies, J. Gaudin, A. Ravasio, E. Brambrink, and A. Benuzzi-Mounaix, Physical Review E 94, 5, 031201 (2016).

[24] E. M. Stolper and T. J. Ahrens, Geophysical Research Letters 14, 1231 (1987).

[25] P. J. Hasnip, K. Refson, M. I. J. Probert, J. R. Yates, S. J. Clark, and C. J. Pickard, Philosophical Transactions of the Royal Society a-Mathematical Physical and Engineering Sciences 372, 26, 20130270 (2014).

[26] Perdew, J.P. and Levy, M., Physical Review Letters, 51(20), 1884-1887, 1983

[27] A. Dewaele, M. Torrent, P. Loubeyre, and M. Mezouar, Physical Review B 78, 13, 104102 (2008).

[28] Kuok and Lim, J. Raman Spectroscopy, 21, 675, 1990

[29] C. Carabatos-Nedelec, F. Brehat, B. Wyncke, Infrared Physics, 31, 611, 1991.

[30] Q. Williams and R. Jeanloz, Physical Review Letters 56, 163 (1986).

[31] A. P. Hammersley, S. O. Svensson, M. Hanfland, A. N. Fitch, and D. Hausermann, High Pressure Research 14, 235 (1996).

[32] C. Prescher and V. B. Prakapenka, High Pressure Research 35, 223 (2015).

[33] A.C., Larson and R.B., Von Dreele , Alamos National Laboratory Report LAUR 86-748. (2004).

[34] G. Kresse and J. Furthmuller, Computational Materials Science 6, 15 (1996).

[35] G. Kresse and J. Furthmuller, Physical Review B 54, 11169 (1996).

[36] P. E. Blochl, Physical Review B 50, 17953 (1994).

[37] G. Kresse and D. Joubert, Physical Review B 59, 1758 (1999).

[38] J. P. Perdew and A. Zunger, Physical Review B 23, 5048 (1981).

[39] J. P. Perdew, K. Burke, and M. Ernzerhof, Physical Review Letters 77, 3865 (1996).

[40] H. Xiao, J. Tahir-Kheli, and W. A. Goddard, Journal of Physical Chemistry Letters 2, 212 (2011).

[41] A. V. Krukau, O. A. Vydrov, A. F. Izmaylov, and G. E. Scuseria, Journal of Chemical Physics 125, 5, 224106 (2006).

[42] A. J. Garza and G. E. Scuseria, Journal of Physical Chemistry Letters 7, 4165 (2016).

[43] H. J. Monkhorst and J. D. Pack, Physical Review B 13, 5188 (1976)

[44] A. R. Oganov, J. P. Brodholt, and G. D. Price, Earth and Planetary Science Letters 184, 555 (2001).

[45] B. K. Godwal, S. Stackhouse, J. Yan, S. Speziale, B. Militzer, and R. Jeanloz, Physical Review B 87, 5, 100101 (2013).

[46] B.G. Hyde, M. O'Keeffe, W.M. Lyttle, and N.E. Brese, Acta Chemica Scandinavica, 46, 216-223 (1992).

[47] W. Jeitschko, Acta Crystallographica Section B-Structural Crystallography and Crystal Chemistry B 24, 930 (1968).

[48] I. Abrahams, and D.Z. Demetriou, Journal of Solid State Chemistry, 149, 28-32 (2000).

[49] R. Jeanloz, Journal of Geophysical Research-Solid Earth and Planets 94, 5873 (1989). [

[50] K. Momma and F. Izumi, Journal of Applied Crystallography, 44, 1272 (2011).

[51] S. Froyen and M.L. Cohen, Journal of Physics-C, Solid State Physics, 19, 2623 (1986).

[52] P. Cervantes, Q. Williams, M. Cote, M. Rohlfing, M.L. Cohen and S.C. Louie, Physical Review B, 58, 9793 (1998).

[53] N.E. Christensen, A. Svane, and E. Peltzer y Blanca, Physical Review B, 72, 014109 (2005).

[54] J.-M. Raulot, G. Baldinozzi, R. Seshadri, and P. Cortona, Solid State Sciences, 4, 467 (2002).

[55] V. V. Sobolev, A. I. Kalugin, and I. V. Vostrikov,

Journal of Surface Investigation-X-Ray Synchrotron and Neutron Techniques 3, 48 (2009).

[56] J. Nara and S. Adachi, Journal of Applied Physics 109, 7, 083539 (2011).

[57] L. Zhang, K. Wang, and B. Zou, The Journal of Physical Chemistry Letters, 11, 4693 (2020)

[58] R. K. Hona, and F, Ramezanipour, Journal of Chemical Sciences, 131, 12039, (2019).

[59] M.R. Filip, G. E. Eperon, H. J. Snaith, and F Guistino, Nature Communications, 5, 5757 (2014).